



## Removal of Cadmium and Lead Ions from Aqueous Solution by Nanocrystalline Magnetite Through Mechanochemical Activation

Mohsen Hosseinzadeh<sup>1</sup>, Seyyed Ali Seyyed Ebrahimi<sup>1</sup>, Shahram Raygan<sup>1</sup>, Seyed Morteza Masoudpanah<sup>2</sup>

<sup>1</sup>Advanced Magnetic Materials Research Center, School of Metallurgy and Materials Engineering, faculty of Engineering, University of Tehran, Tehran, Iran.

<sup>2</sup>School of Metallurgy & Materials Engineering, Iran University of Science and Technology (IUST), Tehran, Iran.

Received: 19 June 2016; Accepted: 11 December 2016

Corresponding author email: [saseyyed@ut.ac.ir](mailto:saseyyed@ut.ac.ir)

### ABSTRACT

In this study, the removal of cadmium and lead ions from aqueous solution by nanocrystalline magnetite was investigated. The nanocrystalline magnetite was synthesized by mechanochemical activation of hematite in a high energy planetary mill in argon atmosphere for 45 hours. The ability of the synthesized nanocrystalline magnetite for removal of Cd(II) and Pb(II) from aqueous solutions was studied in a batch reactor under different experimental conditions with different pHs, contact times, initial metal ion concentrations and temperatures. The solution's pH was found to be a key factor in the adsorption of heavy metal ions on Fe<sub>3</sub>O<sub>4</sub>. The optimum pH of the solution for adsorption of Cd(II) and Pb(II) from aqueous solutions was found to be 6.5 and 5.5, respectively. The best models to describe the kinetics and isotherms of single adsorption were both the pseudo first and second-order kinetic models and Langmuir models, respectively, indicating the monolayer chemisorption of Cd(II) and Pb(II) on Fe<sub>3</sub>O<sub>4</sub> nanoparticles. Moreover, the thermodynamic parameters (i.e.,  $\Delta H^\circ$ ,  $\Delta S^\circ$ ,  $\Delta G^\circ$ ) were evaluated which indicated that the adsorption was spontaneous and exothermic. The results suggested that the synthesized material (magnetite nanocrystalline particles) may be used as effective and economic absorbent for removal of Cd(II) and Pb(II) from aqueous solutions.

**Keywords:** Cadmium ions; Lead ions; Magnetite; Adsorption.

How to cite this article:

Hosseinzadeh M, Seyyed Ebrahimi S A, Raygan S, Masoudpanah S M. Removal of Cadmium and Lead Ions from Aqueous Solution by Nanocrystalline Magnetite Through Mechanochemical Activation. *J Ultrafine Grained Nanostruct Mater*, 2016; 49(2):72-79.

DOI: [10.7508/jufgnsn.2016.02.03](https://doi.org/10.7508/jufgnsn.2016.02.03)

### 1. Introduction

Removal of heavy metal ions, such as Pb(II), Cd(II), As (V) and Hg(II) is one of significant areas for ecological researchers [1]. Up to now, various methods such as chemical precipitation, adsorption, evaporation, ion exchange, membrane filtration, electro dialysis and reverse osmosis, have been developed to treat water containing heavy metals [2–5]. Among them, adsorption has increasingly received much attention in recent years because of

its simple and stable handling process, high efficient wastewater treatment in removing heavy metal ions from wastewaters, absence of secondary pollution and low operating cost [6]. A number of materials including activated carbon [7], bentonite [8] and chitosan [9] have been reported to be capable of adsorbing heavy metal ions from aqueous solutions. Recently, iron oxide especially magnetite [10], hematite [11] and maghemite [12] nanoparticles have been applied to the removal of different heavy

metal ions due to their low cost, environmentally benign nature and excellent adsorption properties for environmental applications [13]. Karami [14] reported that magnetic Fe<sub>3</sub>O<sub>4</sub> nanorods synthesized by pulsed current electrochemical method had the maximum adsorption capacity of 107 and 88 mg/g for Pb(II) and Cd(II) removal from aqueous solutions, respectively. By reducing the diameter of Fe<sub>3</sub>O<sub>4</sub> nanocrystals from 300 to 12 nm, the removal efficiency of As(III) and As(V) increased by orders of magnitude [15].

In this work, the removal capacity of Cd(II) and Pb(II) from aqueous solutions using Fe<sub>3</sub>O<sub>4</sub> nanoparticles prepared by mechanically activation of hematite was systematically investigated and The effects of contact time, initial metal ion concentration and solution pH on the removal of Cd(II) and Pb(II) from aqueous solutions were studied.

## 2. Experimental Procedure

### 2.1. Materials

The raw materials used in the present study were hematite (α-Fe<sub>2</sub>O<sub>3</sub>, Merck, purity>99.5%, grain size of almost 2 μm), cadmium nitrate tetrahyrat (Cd(NO<sub>3</sub>)<sub>2</sub>.4 H<sub>2</sub>O), Merck), lead(II) nitrate(Pb(NO<sub>3</sub>)<sub>2</sub>), Merck), NaOH and HNO<sub>3</sub> with concentration of 0.1 M for adjusting the pH of aqueous solutions and deionized water for making all aqueous solutions. 1000 ppm of Pb(II) and Cd(II) ions stock solution was prepared by dissolving metals salts. The required solutions with different concentrations were made by this stock solution.

### 2.2. Synthesis and characterization of nanocrystalline magnetite

High energy planetary mill (Pulverisette7, Fritsch, Germany) was employed to synthesize nanocrystalline magnetite powder. For this purpose, 12 g hematite was milled in Argon atmosphere for 10, 20 and 45 hours with the powder-to-ball mass ratio of 1:25 in which the balls with the diameter of 3, 5 and 7 mm were used.

X-ray diffraction (XRD) measurements were carried out for phase identification with Philips PW-1730 machine, using CuK<sub>α</sub> radiation. The microstructure of iron oxides was investigated using CAM SCAN MV 2300 scanning electron microscope.

### 2.3. Adsorption studies

Adsorption tests of Cd(II) and Pb(II) using

magnetite nanoparticles were carried out in a batch reactor with the 20 ml of the solution containing 100 ppm of ions and 0.1 g adsorbent. The batch adsorption experiments were conducted to obtain the equilibrium data. A simple magnet was used to separate the magnetite nanoparticles from the solution.

The amount of adsorbed Cd(II) and Pb(II) was calculated from the difference between the initial and final solution concentrations. The concentration of cations in solution was measured by an atomic absorption spectroscope, Varian AA240. The adsorption capacity and removal efficiency of cations were calculated according to the below equations, respectively:

$$q_e = \frac{(C_0 - C_e)V}{m} \quad (\text{eq. 1})$$

$$R \% = \frac{(C_0 - C_e)}{C_0} * 100 \quad (\text{eq. 2})$$

where q<sub>e</sub> (mg/g) is the amount of adsorbed cations onto the unit amount of the adsorbent, C<sub>0</sub> (mg/L) is the initial ion concentration, C<sub>e</sub> (mg/L) is the final or equilibrium ion concentration, V (L) is the volume of the solution, and m (g) is the adsorbent weight in the dry form.

## 3. Results and Discussion

### 3.1. Characterization of mechanically activated hematite

Fig. 1 shows the XRD patterns of as-received hematite (JCPDS file No. 33-0664) and the powders milled for various times. The formation of magnetite (JCPDS file No. 19-0629) began after milling for 10 h and completed for 45 h.

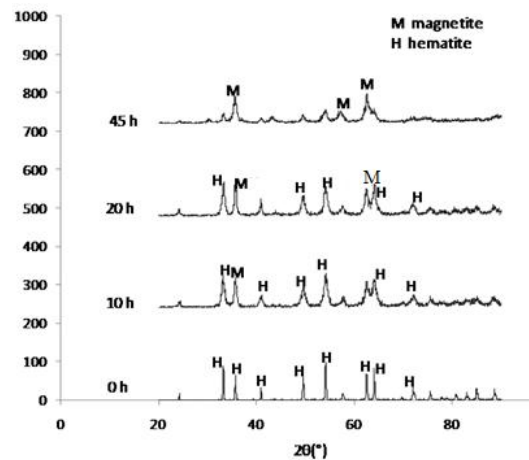


Fig. 1- XRD patterns of the as-received hematite and after milling for different times.

Moreover, milling for more than 45 h has no effect on the phases unless a little oxidation had been appeared. High energy generated during milling is responsible for breaking of the oxygen bonds and reduction of hematite to magnetite without using reducing agents [16, 17].

SEM image of the as-received powder with the particle size of almost 1-2  $\mu\text{m}$  is shown in Fig. 2a. The SEM image of sample milled for 45 hours can also be observed in Fig. 2b. The particle size which determined by the lineal intercept method is about 400 nm with significant agglomeration.

### 3.2. Adsorption batch studies

#### 3.2.1. Adsorption kinetics

Fig. 3a demonstrates the effect of contact time on the adsorption capacity of Pb(II) and Cd(II) on  $\text{Fe}_3\text{O}_4$ . Initially the adsorption amount  $q_t$  increased quickly, then reached equilibria in about 10 and 20 min for the single adsorption of Cd(II) and Pb(II), respectively. The fast adsorption rate at the incipient stage could be attributed to the increase of driving force provided by the concentration gradient of cations in solution and the existence of great number of active sites on the surface of  $\text{Fe}_3\text{O}_4$  nanoparticles [18]. Hence, a contact time of 20 min was sufficient to reach equilibrium for  $\text{Fe}_3\text{O}_4$  nanoparticles in the adsorption of heavy metal ions, which was selected in the further experiments.

In order to understand the characteristics of the adsorption process, three kinetic models, including pseudo-first-order [19], pseudo-second-order [20], and Weber-Morris kinetic models [21] were

applied to fit the experimental data. The expression formulas, the linear forms, the way of plots and the correlative parameters of these kinetic models with the correlation coefficients (R2) were represented in Table 1. The fitting of experimental data to the linear forms for the three adsorption kinetic models were shown in Fig. 3b-d.

The higher linear regression correlations shows the pseudo-first order model and the pseudo-second-order model were more appropriate for describing the single adsorption behavior of Cd(II) and Pb(II). Moreover, the results suggested that both physical and chemical adsorption might be involved in the adsorption behavior of heavy metal ions on  $\text{Fe}_3\text{O}_4$  nanoparticles process [20].

The analysis of Weber–Morris model was applied to discuss the actual rate-controlling step in the single adsorption of Cd(II) and Pb(II), as shown in Fig. 3d. The first line portion represented external mass transfer. The second linear portion which shows intra-particle diffusion, is sorption. The plots did not through the origin, suggesting that intra-particle diffusion was not the only rate-controlling step, and the external mass transfer also contributed significantly in the rate-controlling step due to the large intercepts of the second linear portion of the plots. So the adsorption process was collectively controlled by external mass transfer and intra-particle diffusion [21].

#### 3.2.2. Adsorption isotherm

To explore the adsorption capacities of  $\text{Fe}_3\text{O}_4$  nanoparticles toward Cd(II) and Pb(II), the

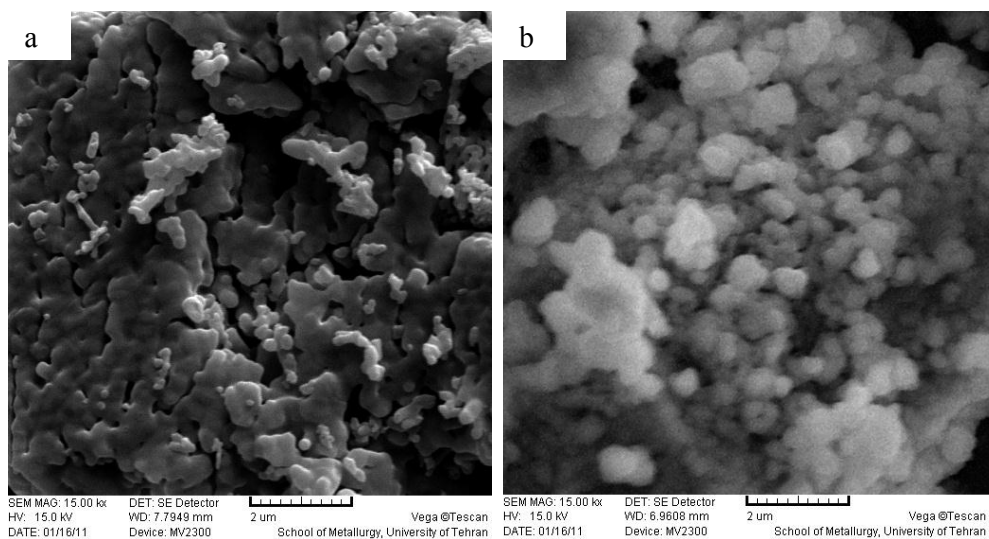


Fig. 2- The SEM images of a) hematite (as-received) and b) after milling for 45 h.

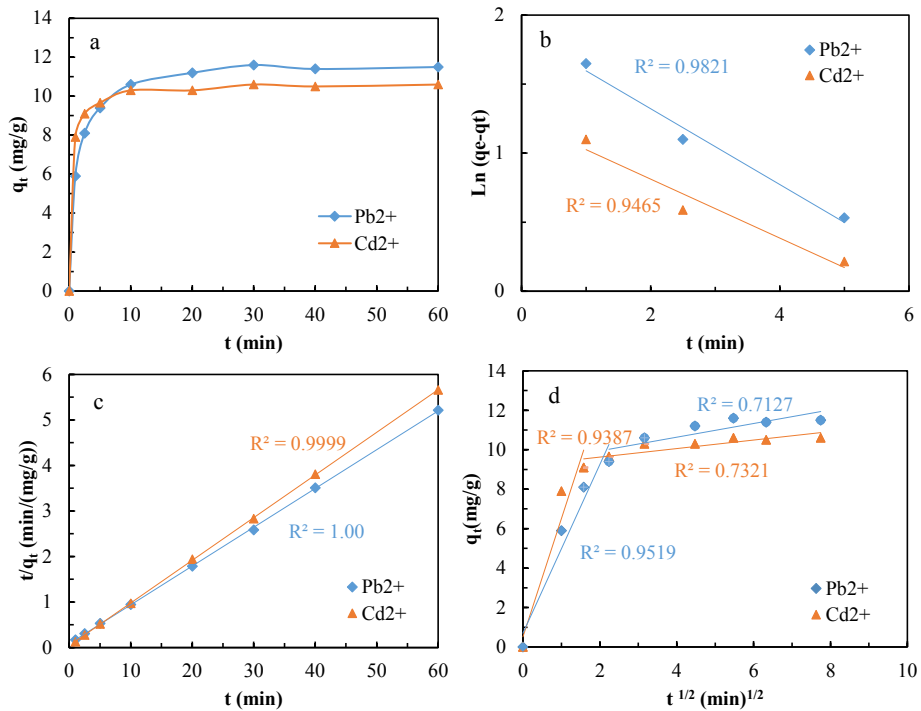


Fig. 3- (a) Adsorption kinetics of phosphate on Fe<sub>3</sub>O<sub>4</sub> using (b) Pseudo-first order, (c) Pseudo-second order and (d) Weber-Morris models (adsorption dose, 5 g/L, initial cation concentration, 100 mg/L, contact time, 20 min, and adsorption temperature, 25 °C).

adsorption of metal ions with different initial concentrations (50-200 mg/L) was investigated. Fig. 4a shows single adsorption isotherms with the initial concentrations ranging from 50 to 250 mg/L. It was observed that the adsorption amount of Fe<sub>3</sub>O<sub>4</sub> nanoparticles increased gradually at low concentrations (0–100 mg/L), then reached a plateau and steady stayed for higher initial concentrations of metal ions.

The adsorption data of Fe<sub>3</sub>O<sub>4</sub> nanoparticles were analyzed using three different isothermal adsorption models, namely Langmuir model [22], Freundlich model [23] and Dubinin-Radushkevich (D-

R) model [24], respectively (Fig. 4b-d), and the calculated isothermal parameters were presented in Table 2. Compared with the Freundlich and Dubinin-Radushkevich models, the Langmuir model fitted better with the experimental data due to the higher correlation coefficients ( $R^2 > 0.999$ ).

The maximum adsorption capacities calculated by the Langmuir model were 13.8 and 9.52 mg/g, for Cd(II) and Pb(II), respectively, which were rather close to the values experimentally determined (12.6 and 9.01 mg/g) in Fig. 4a. As documented, the Langmuir model assumes monolayer coverage of the adsorbent surface, on which the binding

Table 1- Adsorption kinetic models, the corresponding linear forms and parameters of Fe<sub>3</sub>O<sub>4</sub> obtained at three phosphate initial concentrations

| Kinetic models      | Linear form   | Parameters                    | Pb(II) | Cd(II) |
|---------------------|---|-------------------------------|--------|--------|
| Pseudo-first order  | $\ln(q_e - q_t) = \ln q_e - k_1 t$                      | $q_e$ (mg g <sup>-1</sup> )   | 3.45   | 6.48   |
|                     |   | $K_1$ (min <sup>-1</sup> )    | 0.274  | 0.213  |
| Pseudo-second-order | $\frac{t}{q_t} = \frac{1}{k_2 q_e^2} + \frac{1}{q_e} t$ | $q_e$ (mg g <sup>-1</sup> )   | 11.11  | 10.6   |
|                     |   | $K_2$ (min <sup>-1</sup> )    | 0.090  | 0.214  |
| Weber-Morris        | $q_t = k_{d1} t^{0.5} + c$                              | $K_{d1}$ (min <sup>-1</sup> ) | 4.278  | 5.989  |
|                     |   | $K_{d2}$ (min <sup>-1</sup> ) | 0.347  | 0.215  |

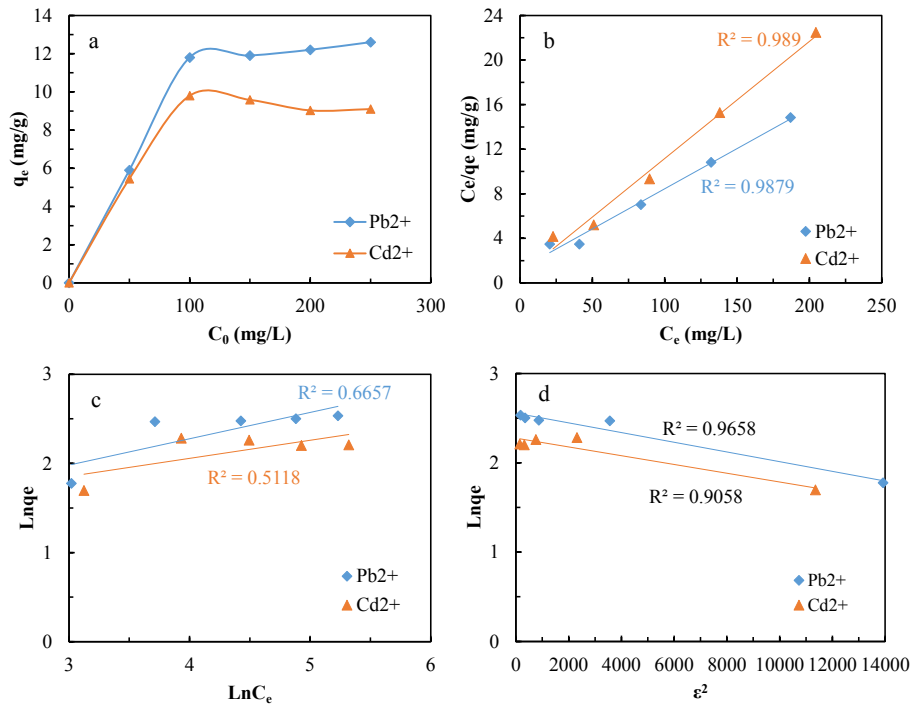


Fig. 4- (a) Adsorption isotherms, (b) Langmuir, (c) Freundlich, and (d) Dubinin-Radushkevich isotherm plots for adsorption of Cd(II) and Pb(II) on Fe<sub>3</sub>O<sub>4</sub> nanoparticles (Adsorption dose, 5 g/L, pH, 5.5, contact time, 20 min, and adsorption temperature, 25 °C).

sites have the same affinity for the adsorption [22]. Therefore, the formed monolayer was possibly due to the chemical interaction between Fe<sub>3</sub>O<sub>4</sub> nanoparticles and heavy metal ions.

The conformity of adsorption data to the Langmuir isotherm ( $R^2 \approx 1.00$ ) could be interpreted as a homogeneous adsorption process, leading to a monolayer binding. The equilibrium parameter (RL values) in the range of  $0 < RL < 1$  indicated that the adsorbent was much more favorable (see Table 2). The results well agreed with the observations of

previous reports for the adsorption of Pb(II) and Cd(II) ions onto the other adsorbents [25, 26]. However, according to the analysis of the D–R model, the E values was about 1.0 kJ/mol, which indicated that the adsorption behavior of Pb(II) and Cd(II) ions on Fe<sub>3</sub>O<sub>4</sub> could be described as the weak interaction of cations with this adsorbent [22].

### 3.2.3. Adsorption thermodynamics

The effect of temperature is a major influencing factor in the adsorption process. The dependence of

Table 2- Adsorption isotherm models, the corresponding linear forms and parameters of Fe<sub>3</sub>O<sub>4</sub> obtained with pH 5.5 at 25 °C

| Isotherm models | Linear form   | Parameters                               | Pb(II)             | Cd(II)             |
|-----------------|---|--|--------------------|--------------------|
| Langmuir        | $\frac{C_e}{q_e} = \frac{1}{q_m b} + \frac{C_e}{q_m}$   | $q_m$ (mg g <sup>-1</sup> )              | 13.88              | 9.52               |
|                 |   | $b$ (L mg <sup>-1</sup> )                | 0.058              | 0.156              |
|                 |   | $R_L = \frac{1}{1 + bC_0}$               | 0.05-0.2           | 0.05-0.2           |
| Freundlich      | $Lnq_e = Lnk_F + \frac{1}{n}LnC_e$  | $k_F$ (L g <sup>-1</sup> )               | 2.99               | 3.46               |
| D-R             | $Lnq_e = Lnq_{mD} - B\varepsilon^2$<br>$\varepsilon = RTLn(1 + \frac{1}{C_e})$<br>$E = -(2B)^{0.5}$ | $n$                                      | 3.38               | 4.92               |
|                 |   | $q_{mD}$ (mg g <sup>-1</sup> )           | 12.88              | 10.07              |
|                 |   | $B$ (mol <sup>2</sup> kJ <sup>-2</sup> ) | $5 \times 10^{-5}$ | $5 \times 10^{-5}$ |
|                 |   | $E$ (J/mol)                              | -100               | -100               |

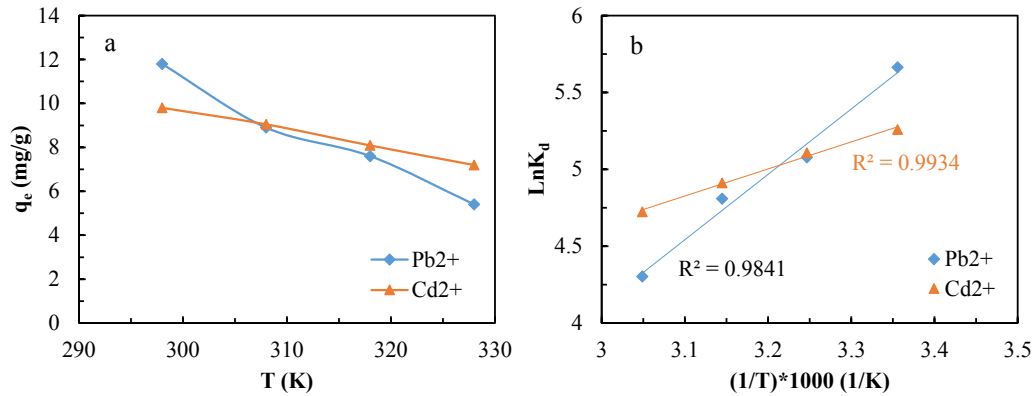


Fig. 5- (a) Adsorption thermodynamics and (b)  $\ln K_d$  vs.  $(1/T) \times 10^3$  plots for adsorption of Cd(II) and Pb(II) on  $Fe_3O_4$  nanoparticles (Adsorption dose, 5 g/L, pH, 5.5, and contact time, 20 min).

the adsorption capacity as a function of adsorption temperature is shown in Fig. 5a. The adsorption on the magnetite adsorbent decreased with increasing of the adsorption temperature. This decrease indicates that the adsorption is not favorable at higher temperatures and adsorption process is exothermic [27]. The thermodynamic parameters ( $\Delta H^\circ$ ,  $\Delta S^\circ$ , and  $\Delta G^\circ$ ) for adsorption on  $Fe_3O_4$  can be calculated from the temperature dependent adsorption. The values of enthalpy and entropy changes ( $\Delta H^\circ$  and  $\Delta S^\circ$ ) can be calculated from the slope and y-intercept of the plot of  $\ln K_d$  vs.  $1/T$  via applying the following equations [28]:

$$\Delta G^\circ = \Delta H^\circ - T\Delta S^\circ \quad (\text{eq. 3})$$

$$\ln K_d = \frac{\Delta S^\circ}{R} - \frac{\Delta H^\circ}{RT} \quad (\text{eq. 4})$$

$$K_d = \frac{C_0 - C_e}{C_e} \frac{V}{m} \quad (\text{eq. 5})$$

Where  $K_d$  is equilibrium distribution coefficient,  $C_0$  (mg/l) is the initial concentration,  $C_e$  (mg/l) is the equilibrium concentration,  $V$  is the volume (mL),  $m$  is the mass of the powder (g),  $R$  (8.314 J/mol K) is the ideal gas constant, and  $T$  (K) is the temperature. The estimated thermodynamic parameters shown in Table 3 are in the agreement with other reported

data. Duan et al. reported the enthalpy change  $\Delta H^\circ$  of 14.53 kJ/mol, entropy change  $\Delta S^\circ$  of 58.20 J/mol.K for adsorption of  $Pb^{2+}$  on the cobalt doped magnetite powders [29]. Accordingly, Boparai et al. also obtained  $\Delta H^\circ$  of 7.17 kJ/mol and  $\Delta S^\circ$  of 45.3 J/mol.K for adsorption of  $Cd^{2+}$  on zerovalent iron particles [30]. The distribution coefficient  $K_d$  values decreased with raising temperature (Fig. 5b), indicating the exothermic nature of adsorption.

The negative value of  $\Delta S^\circ$  for the adsorption can be attributed to the ordering at the solid/solution interface and a decrease in the degree of freedom of the adsorbed species. The negative values of  $\Delta G^\circ$  indicate feasibility of adsorption of metal ions on the adsorbent. Moreover, the  $\Delta G^\circ$  values obtained in this study for Pb(II) and Cd(II) ions were  $< -20$  kJ/mol, suggesting that the physical adsorption mechanism existed in the adsorption process [18]. This was in accordance with the analysis of D-R isotherm model.

### 3.2.4. pH

The pH of the initial solution plays an important role for adsorption experiments. The effects of pH on the adsorption capacity of cations by the milled powder are shown in Fig. 6. The adsorption

Table 3- Thermodynamic parameters obtained at different temperatures during adsorption on  $Fe_3O_4$

| T(K) | $\Delta G^\circ$ (kJmol <sup>-1</sup> ) |        | $\Delta H^\circ$ (kJmol <sup>-1</sup> ) |        | $\Delta S^\circ$ (Jmol <sup>-1</sup> K <sup>-1</sup> ) |        |
|------|---|--------|---|--------|--|--------|
|      | Pb(II)                                  | Cd(II) | Pb(II)                                  | Cd(II) | Pb(II)   | Cd(II) |
| 298  | -14.03                                  | -13.03 | -35.3                                   | -14.6  | -71.7  | -5.2   |
| 308  | -13.00                                  | -13.08 |   |        |  |        |
| 318  | -12.71                                  | -13.00 |   |        |  |        |
| 328  | -11.73                                  | -12.88 |   |        |  |        |

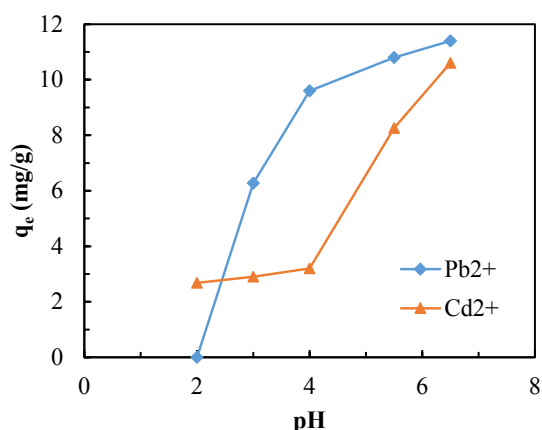
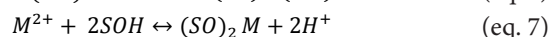
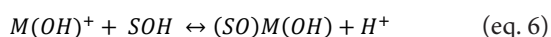


Fig. 6- Effect of pH on adsorption of Cd(II) and Pb(II) by Fe<sub>3</sub>O<sub>4</sub> nanoparticles (amount of adsorbent: 5g/l; initial concentration, 100 mg/l; contact time 20 min; temperature 25 °C).

capacities of Pb(II) and Cd(II) cations increased with the increase of initial pH. However, in order to prohibit from precipitating in the form of metal hydroxides for higher pH's, the pH values higher than 6.5 and 7 were not preferred for Pb(II) and Cd(II), respectively [15,18]. At lower initial pH values, H<sup>+</sup> compete with the cations for the surface binding sites of the adsorbent, while with increasing the pH and decreasing the competing effect of H<sup>+</sup> ions, the positively charged cations species occupied the free binding sites [31]. Moreover, the pH of the solution decreased after adsorption of the cations which can be attributed to the replacement of surface protons by adsorbed metal cations, according to the following tentative mechanisms [32]:



For these reactions, SOH and M signify adsorbent and adsorbed metal, respectively.

#### 4. Conclusions

Magnetite Fe<sub>3</sub>O<sub>4</sub> nanoparticles synthesized by mechanical activation were used to remove Pb(II) and Cd(II) from aqueous solutions. Batch adsorption experiments were carried out at different contact times, initial concentrations of heavy metal ions and pH values, respectively. It was found that the adsorption rates were very fast and adsorption equilibria were obtained in about 10 and 20 min for the adsorption of Cd(II) and Pb(II), respectively. The best models to describe the kinetics and isotherms of single adsorption were both the pseudo first and second-order

kinetic models and Langmuir models, respectively, indicating the monolayer chemisorption of Cd(II) and Pb(II) on Fe<sub>3</sub>O<sub>4</sub> nanoparticles. Thermodynamic parameters revealed that the nature of adsorption was spontaneous and exothermic. Moreover, the solution pH was found to be a key factor in the adsorption of heavy metal ions on Fe<sub>3</sub>O<sub>4</sub>.

#### References

1. Fu F, Wang Q. Removal of heavy metal ions from wastewaters: a review. *Journal of Environmental Management*. 2011;92(3):407-18.
2. Esalah JO, Weber ME, Vera JH. Removal of lead, cadmium and zinc from aqueous solutions by precipitation with sodium Di-(n-octyl) phosphinate. *The Canadian Journal of Chemical Engineering*. 2000;78(5):948-54.
3. An HK, Park BY, Kim DS. Crab shell for the removal of heavy metals from aqueous solution. *Water Research*. 2001;35(15):3551-6.
4. Kumar KY, Muralidhara HB, Nayaka YA, Balasubramanyam J, Hanumanthappa H. Hierarchically assembled mesoporous ZnO nanorods for the removal of lead and cadmium by using differential pulse anodic stripping voltammetric method. *Powder Technology*. 2013;239:208-16.
5. Mahmood T, Saddique MT, Naem A, Mustafa S, Dilara B, Raza ZA. Cation exchange removal of Cd from aqueous solution by NiO. *Journal of Hazardous Materials*. 2011;185(2):824-8.
6. Xiong C, Wang W, Tan F, Luo F, Chen J, Qiao X. Investigation on the efficiency and mechanism of Cd (II) and Pb (II) removal from aqueous solutions using MgO nanoparticles. *Journal of Hazardous Materials*. 2015;299:664-74.
7. Olowoyo DN, Garuba AO. Adsorption of Cadmium Ions using activated carbon prepared from Coconut shell. *Global Advanced Research Journal of Food Science and Technology*. 2012;1(6):81-4.
8. Futralan CM, Kan CC, Dalida ML, Hsien KJ, Pascua C, Wan MW. Comparative and competitive adsorption of copper, lead, and nickel using chitosan immobilized on bentonite. *Carbohydrate Polymers*. 2011;83(2):528-36.
9. Zhu Y, Hu J, Wang J. Competitive adsorption of Pb (II), Cu (II) and Zn (II) onto xanthate-modified magnetic chitosan. *Journal of Hazardous Materials*. 2012;221:155-61.
10. Feng L, Cao M, Ma X, Zhu Y, Hu C. Superparamagnetic high-surface-area Fe<sub>3</sub>O<sub>4</sub> nanoparticles as adsorbents for arsenic removal. *Journal of Hazardous Materials*. 2012;217:439-46.
11. Shan C, Ma Z, Tong M. Efficient removal of trace antimony (III) through adsorption by hematite modified magnetic nanoparticles. *Journal of Hazardous Materials*. 2014;268:229-36.
12. Roy A, Bhattacharya J. Removal of Cu (II), Zn (II) and Pb (II) from water using microwave-assisted synthesized maghemite nanotubes. *Chemical Engineering Journal*. 2012;211:493-500.
13. Ngomsik AF, Bee A, Draye M, Cote G, Cabuil V. Magnetic nano- and microparticles for metal removal and environmental applications: a review. *Comptes Rendus Chimie*. 2005;8(6):963-70.
14. Karami H. Heavy metal removal from water by magnetite nanorods. *Chemical Engineering Journal*. 2013;219:209-16.
15. Morillo D, Pérez G, Valiente M. Efficient arsenic (V) and arsenic (III) removal from acidic solutions with Novel Forager Sponge-loaded superparamagnetic iron oxide nanoparticles. *Journal of Colloid and Interface Science*. 2015;453:132-41.
16. Zdujic M, Jovalekić Č, Karanović L, Mitrić M, Poletić D, Skala D. Mechanochemical treatment of α-Fe<sub>2</sub>O<sub>3</sub> powder

- in air atmosphere. *Materials Science and Engineering: A*. 1998;245(1):109-17.
17. Zdujić M, Jovalekić Č, Karanović L, Mitrić M. The ball milling induced transformation of  $\alpha$ - $\text{Fe}_2\text{O}_3$  powder in air and oxygen atmosphere. *Materials Science and Engineering: A*. 1999;262(1):204-13.
  18. Nassar NN. Rapid removal and recovery of Pb (II) from wastewater by magnetic nanoadsorbents. *Journal of Hazardous Materials*. 2010;184(1):538-46.
  19. Ngah WW, Fatinathan S. Adsorption characterization of Pb (II) and Cu (II) ions onto chitosan-tripolyphosphate beads: kinetic, equilibrium and thermodynamic studies. *Journal of Environmental Management*. 2010;91(4):958-69.
  20. Cheknane B, Zermane F, Baudu M, Bouras O, Basly JP. Sorption of basic dyes onto granulated pillared clays: Thermodynamic and kinetic studies. *Journal of Colloid and Interface Science*. 2012;381(1):158-63.
  21. Liu X, Zhang L. Removal of phosphate anions using the modified chitosan beads: adsorption kinetic, isotherm and mechanism studies. *Powder Technology*. 2015;277:112-9.
  22. Vijaya Y, Popuri SR, Boddu VM, Krishnaiah A. Modified chitosan and calcium alginate biopolymer sorbents for removal of nickel (II) through adsorption. *Carbohydrate Polymers*. 2008;72(2):261-71.
  23. Kamari A, Ngah WW. Isotherm, kinetic and thermodynamic studies of lead and copper uptake by H<sub>2</sub>SO<sub>4</sub> modified chitosan. *Colloids and Surfaces B: Biointerfaces*. 2009;73(2):257-66.
  24. Al-Haidary AM, Zanganah FH, Al-Azawi SR, Khalili FI, Al-Dujaili AH. A study on using date palm fibers and leaf base of palm as adsorbents for Pb (II) ions from its aqueous solution. *Water, Air, & Soil Pollution*. 2011;214(1-4):73-82.
  25. Meena AK, Kadirvelu K, Mishraa GK, Rajagopal C, Nagar PN. Adsorption of Pb (II) and Cd (II) metal ions from aqueous solutions by mustard husk. *Journal of Hazardous Materials*. 2008;150(3):619-25.
  26. Mehta D, Mazumdar S, Singh SK. Magnetic adsorbents for the treatment of water/wastewater—a review. *Journal of Water Process Engineering*. 2015;7:244-65.
  27. Yanagisawa H, Matsumoto Y, Machida M. Adsorption of Zn (II) and Cd (II) ions onto magnesium and activated carbon composite in aqueous solution. *Applied Surface Science*. 2010;256(6):1619-23.
  28. Sheng G, Wang S, Hu J, Lu Y, Li J, Dong Y, Wang X. Adsorption of Pb (II) on diatomite as affected via aqueous solution chemistry and temperature. *Colloids and Surfaces A: Physicochemical and Engineering Aspects*. 2009;339(1):159-66.
  29. Duan S, Tang R, Xue Z, Zhang X, Zhao Y, Zhang W, Zhang J, Wang B, Zeng S, Sun D. Effective removal of Pb (II) using magnetic  $\text{Co}_{0.6}\text{Fe}_{2.4}\text{O}_4$  micro-particles as the adsorbent: Synthesis and study on the kinetic and thermodynamic behaviors for its adsorption. *Colloids and Surfaces A: Physicochemical and Engineering Aspects*. 2015;469:211-23.
  30. Boparai HK, Joseph M, O'Carroll DM. Kinetics and thermodynamics of cadmium ion removal by adsorption onto nano zerovalent iron particles. *Journal of Hazardous Materials*. 2011;186(1):458-65.
  31. Jiang MQ, Jin XY, Lu XQ, Chen ZL. Adsorption of Pb (II), Cd (II), Ni (II) and Cu (II) onto natural kaolinite clay. *Desalination*. 2010;252(1):33-9.
  32. Komárek M, Koretsky CM, Stephen KJ, Alessi DS, Chrastny V. Competitive Adsorption of Cd (II), Cr (VI), and Pb (II) onto Nanomaghemite: A Spectroscopic and Modeling Approach. *Environmental Science & Technology*. 2015;49(21):12851-9.



